



**HAL**  
open science

# Analysis of an Inverter-Based CMOS Envelope Detector

Jack Ou, Pietro Maris Ferreira

► **To cite this version:**

Jack Ou, Pietro Maris Ferreira. Analysis of an Inverter-Based CMOS Envelope Detector. IEEE International Conference on Electronics, Circuits and Systems, Oct 2022, Glasgow, United Kingdom. hal-03799138

**HAL Id: hal-03799138**

**<https://hal.science/hal-03799138v1>**

Submitted on 5 Oct 2022

**HAL** is a multi-disciplinary open access archive for the deposit and dissemination of scientific research documents, whether they are published or not. The documents may come from teaching and research institutions in France or abroad, or from public or private research centers.

L'archive ouverte pluridisciplinaire **HAL**, est destinée au dépôt et à la diffusion de documents scientifiques de niveau recherche, publiés ou non, émanant des établissements d'enseignement et de recherche français ou étrangers, des laboratoires publics ou privés.

# Analysis of an Inverter-Based CMOS Envelope Detector

Jack Ou

Department of Electrical and Computer Engineering  
California State University Northridge  
Northridge, California 91330-8346  
Email: jack.ou@csun.edu

Pietro M. Ferreira

GeePs (UMR CNRS 8507)  
CentraleSupélec, Université Paris-Saclay  
Gif-sur-Yvette, France  
Email: maris@ieee.org

**Abstract**—This article derives the scaling factor of a sub-threshold inverter-based envelope detector. The scaling factor was simulated at the transistor-level using BSIM4 model parameters in 180 nm CMOS. A close analysis of the the calculated scaling factor shows that the minimum and the maximum of the scaling factor are within 10 percent of those obtained in simulation, suggesting that the scaling factor of the inverter-based envelope detector biased in the subthreshold region is accurately modeled.

## I. INTRODUCTION

Recent studies have shown that by 2027 battery powered Internet of Things (IoT) devices will become ubiquitous [1]. In order to minimize battery usage and prolong battery life, it will be necessary to develop energy efficient wake-up receivers (WuRx) that monitor wireless channel continuously and turn on the battery powered devices on demand.

Despite recent efforts to shorten the wake-up receiver design cycle, WuRx circuits have always been associated with limited portability across technology nodes and required significant time and effort in design, optimization, custom layout, and prototyping. Consequently, there continues to be strong interests in developing digital-friendly WuRx circuits, i.e. WuRx circuits built with digital gates.

The power consumption of wake-up receivers can be significantly reduced by using an envelope detector which eliminates the need for RF amplification and generation of LO frequency [2]. Figure 1(a) shows the inverter-based CMOS envelope detector first reported in [3]. In contrast to prior envelope-detector designs which utilized distortion in elementary amplifiers such as a common-drain amplifier [4], a common-gate amplifier [5], and a common-source amplifier [6], the inverter-based envelope detector uses the second order distortion current generated by an inverter biased in the subthreshold region to generate conversion gain [3]. The conversion gain is maximized with the transistors biased in the subthreshold region. The conversion gain is sensitive to small variations of the gate bias voltage [3]. [3] showed that by using a charge-scaling digital-to-analog conversion (DAC) circuit to generate the gate bias voltage, the circuit's sensitivity to the gate bias voltage is mitigated.

[3] shows that it is feasible to generate conversion gain with a digital inverter, but does not describe the underlying

theoretical framework for generating the conversion gain. This article addresses the knowledge gap by deriving the voltage transfer characteristic (VTC), the small signal gain, and the scaling factor of the inverter-based envelope detector biased in the subthreshold region.

The VTC relates the output voltage of an inverter to its input voltage. The VTC is derived in this article to account for the dependence of the threshold voltage on the drain-to-source voltage through the drain-induced barrier lowering (DIBL) effect. In contrast to the VTC expression derived in [7], the VTC expression produces a gradual descent near  $V_S$ , the switching voltage at which the input voltage is equal to the output voltage, and accurately models the small signal gain.

The first derivative of the output voltage with respect to the input voltage is the small signal gain ( $A_V$ ).  $A_V$  can be computed at any point along the VTC. In contrast to  $A_V$  derived in [8], the  $A_V$  derived in this article is valid not only near the switching voltage, but also for any output voltage and can be used along with the VTC expression to compute the small signal gain as a function of the input voltage. More importantly, since the minimum and the maximum of second derivative of the voltage transfer function occur away from the switching voltage, a general small signal gain expression valid for any input voltage is needed to calculate the scaling factor or the conversion gain of the envelope detector.

The second derivative of the output voltage with respect to the input voltage gives rise to the scaling factor and the voltage conversion gain of the envelope detector (Sec. II-B). Analytical expressions for the scaling factor and the voltage conversion gain are derived in this article. The expressions are valid for any input voltage and can be evaluated along with the VTC expression and the general small signal expression to compute the scaling factor and the voltage conversion gain for an inverter-based envelope detector biased in the subthreshold region.

The close agreement between the simulated and the calculated of the second derivative of the voltage transfer characteristic curve shows that the voltage conversion gain for an inverter-based envelope detector biased in the subthreshold region is accurately modeled.

The article is organized as follows: Section II provides definitions, background, and preliminary simulation results for

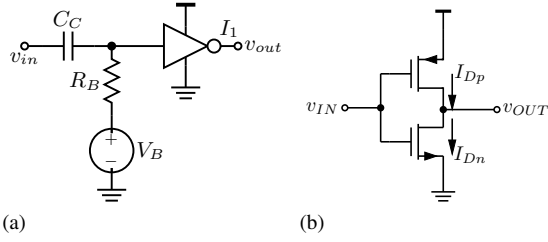


Fig. 1. (a) The simplified schematic of the inverter-based envelope detector. (b) Transistor-level implementation of the inverter cell.

understanding the operation of the inverter-based envelope detector in subthreshold region. Section III describes the derivation of expressions for voltage transfer characteristic, small signal gain, and scaling factor for the envelope detector. Section IV compares the simulated VTC, simulated small signal gain, and the simulated scaling factor with calculations using expressions derived in Sec. III. Conclusions are summarized in Sec. V

## II. BACKGROUND

### A. Distortion Characteristics of the Inverter Cell

Figure 1(a) is a simplified schematic of the inverter-based envelope detector.  $C_C$  is a coupling capacitor.  $R_B$  is implemented with an NMOS transistor biased in the subthreshold region.  $V_B$  is an adjustable DC voltage source discussed in [3]. Figure 1(b) shows the transistor level implementation of the inverter circuit.

### B. Definitions

For weakly nonlinear CMOS inverters, the output voltage ( $v_{OUT}$ ) can be approximated by the Taylor series expansion as

$$v_{OUT} = V_{OUT} + \frac{dV_{OUT}}{dV_{IN}} v_{in} + \frac{d^2 V_{OUT}}{dV_{IN}^2} \frac{v_{in}^2}{2}. \quad (1)$$

Let  $v_{in}$  be an amplitude modulated input,

$$v_{in} = v_m(1 + k_a m(t)) \cos \omega_c t. \quad (2)$$

$v_m$  is the amplitude of the carrier wave and  $\omega_c$  is the angular frequency of the carrier wave.  $k_a$  is the amplitude sensitivity of the modulator. For single tone modulation,  $m(t) = A_m \cos \omega_m t$ . The amplitude of baseband signal at the output of the inverter-based envelope detector is

$$v_{out,bb} = \frac{d^2 V_{OUT}}{dV_{IN}^2} \frac{v_m^2 \mu}{2}, \quad (3)$$

where  $\mu$  is the modulation index and is equal to  $k_a A_m$ . For  $\mu = 1$ , the voltage conversion gain ( $G_V$ ) of the inverter-based envelope detector is

$$G_V = \frac{v_{out,bb}}{v_m} = \frac{d^2 V_{OUT}}{dV_{IN}^2} \frac{v_m}{2} \quad (4)$$

and the scaling factor  $k$  of is

$$k = \frac{v_{out,bb}}{v_m^2} = \frac{d^2 V_{OUT}}{dV_{IN}^2} \frac{1}{2}. \quad (5)$$

$G_V$  is dependent on  $v_m$  while  $k$  is independent of  $v_m$ .

### C. Prior Work

Figure 2(a) shows the second derivative of  $V_{OUT}$  with respect to  $V_{IN}$ . The minimum of the second derivative occurs at just below  $V_S$  while the maximum of the second derivative occurs above  $V_S$ . Figure 2(a) suggests that  $k$  and  $G_V$  are higher with  $V_{DD}$  at 0.5 V. This observation is consistent with the observations reported in [3] which showed that  $k$  and  $G_V$  are maximized and the current consumption is reduced when the transistors operate in the subthreshold region. Figure 2(b) shows the sensitivity of the second derivative of  $V_{OUT}$  with respect to  $V_{IN}$  to process corners. [3] showed that by using a charge-scaling digital-analog converter circuit to adjust the gate bias voltage ( $V_B$ ) in small increments, the circuit's sensitivity to process corners can be mitigated.

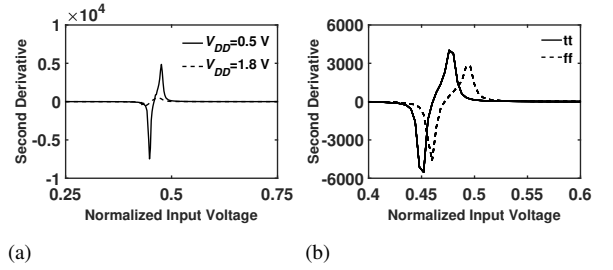


Fig. 2. (a) The second derivative as a function of the normalized  $V_{IN}$  and  $V_{DD}$ . (b) The second derivative of the voltage transfer function as a function of process corners and the normalized input voltage for  $V_{DD}$  of 0.5 V.

## III. ANALYSIS OF AN INVERTER-BASED ENVELOPE DETECTOR

### A. Transistor Model in Subthreshold Region

For NMOS transistors operating in the subthreshold region, the drain current is [8]

$$I_{Dn} = I_{on} e^{\frac{V_{GS} - V_{tn}}{n_n V_T}} (1 - e^{-\frac{V_{DS}}{V_T}}). \quad (6)$$

$V_{GS}$  is the gate-to-source voltage.  $V_{DS}$  is the drain-to-source voltage.  $V_T = kT/q$  is the thermal voltage.  $n_n$  is the subthreshold slope factor.  $I_{on}$  is a technology-dependent parameter

$$I_{on} = (n_n - 1) \frac{W_n}{L_n} \mu_n C_{ox} V_T^2, \quad (7)$$

where  $W_n/L_n$  is the aspect ratio,  $\mu_n$  is the electron mobility, and  $C_{ox}$  is the oxide capacitance.  $V_{tn}$  is the threshold voltage and can be expressed as [8]

$$V_{tn} = V_{tn0} - \lambda_{DSn} V_{DS} - \lambda_{BSn} V_{BS} \quad (8)$$

$V_{tn0}$  is the zero-bias threshold voltage (i.e., the value extracted under  $V_{DS} = V_{BS} = 0$  V, whereas  $\lambda_{DSn}$  and  $\lambda_{BSn}$  are positive technology-dependent coefficients.  $V_{BS}$  is the body-to-source voltage.

Equation (6) can be used to model PMOS transistors in the subthreshold region by replacing  $V_{GS}$  with  $|V_{GS}|$ ,  $V_{DS}$  with  $|V_{DS}|$ ,  $I_{Dn}$  with  $|I_{Dp}|$ ,  $n_n$  with  $n_p$ ,  $V_{tn}$  with  $|V_{tp}|$ ,  $I_{on}$  with  $I_{op}$ , and  $\lambda_{DSn}$  with  $\lambda_{DSp}$ .

## B. Voltage Transfer Characteristic

The VTC of the inverter-based envelope detector in Fig. 1(b) can be obtained by setting  $I_{Dp}$  equal to  $I_{Dn}$  in Fig. 1(b), replacing  $V_{GS}$  and  $V_{DS}$  of the NMOS with  $V_{IN}$  and  $V_{OUT}$ , respectively, and replacing  $|V_{GS}|$  and  $|V_{DS}|$  of the PMOS with  $V_{DD} - V_{IN}$  and  $V_{DD} - V_{OUT}$ . The VTC is

$$I_S e^{\frac{V_{IN}}{n_{eff} V_T}} = \frac{1 - e^{-\frac{V_{DD} - V_{OUT}}{V_T}}}{1 - e^{-\frac{V_{OUT}}{V_T}}}, \quad (9)$$

where  $I_S$  and  $n_{eff}$  are

$$I_S = \frac{I_{on}}{I_{op}} e^{-\frac{V_{DD}}{n_p V_T} - \frac{V_{tn}}{n_n V_T} + \frac{|V_{tp}|}{n_p V_T}} \quad (10)$$

and

$$\frac{1}{n_{eff}} = \frac{1}{n_n} + \frac{1}{n_p} \quad (11)$$

The dependence of (9) on  $\lambda_{DSn}$  and  $\lambda_{DSp}$  can be explicitly expressed by 1) replacing  $V_{tn}$  (and  $V_{tp}$ ) with (8) and 2) simplifying the resulting equation,

$$I_{So} e^{\frac{V_{IN}}{n_{eff} V_T}} = \frac{1 - e^{-\frac{V_{DD} - V_{OUT}}{V_T}}}{1 - e^{-\frac{V_{OUT}}{V_T}}} e^{-(\frac{\lambda_{DSn}}{n_n} + \frac{\lambda_{DSp}}{n_p}) \frac{V_{OUT}}{V_T}}, \quad (12)$$

where

$$I_{So} = \frac{I_{on}}{I_{op}} e^{-\frac{V_{DD}}{n_p V_T}} e^{-(\frac{V_{tnp}}{n_n V_T} - \frac{|V_{tpo}|}{n_p V_T})} e^{-\frac{\lambda_{DSp} V_{DD}}{n_p V_T}}. \quad (13)$$

$I_{So}$  is independent of  $V_{IN}$  and  $V_{OUT}$  but is a function of  $V_{DD}$ . In contrast to the VTC derived in [7], (12) accounts for the DIBL effect, yields a gradual descent near  $V_S$  and accurately captures  $A_V$ .

## C. Small Signal Voltage Gain

$A_V$ , the small signal voltage gain of the inverter-based envelope detector, is obtained by differentiating both sides of (12) with respect to  $V_{IN}$ , approximating  $n_n$  and  $n_p$  as  $n$ , and rearranging the resulting equation as

$$\frac{-1}{A_V} = \lambda_{DS} + \frac{n}{2} \frac{e^{-\frac{V_{DD} - V_{OUT}}{V_T}}}{1 - e^{-\frac{V_{DD} - V_{OUT}}{V_T}}} + \frac{n}{2} \frac{e^{-\frac{V_{OUT}}{V_T}}}{1 - e^{-\frac{V_{OUT}}{V_T}}}, \quad (14)$$

where  $\lambda_{DS} = \frac{\lambda_{DSn} + \lambda_{DSp}}{2}$ . In contrast to the small signal gain derived in [8], (14) is valid not only near  $V_S$ , but also for any  $V_{OUT}$  and can be used along with (12) to compute  $A_V$  as a function of  $V_{IN}$ . More importantly, since the minimum and the maximum of  $A_V$  occur away from  $V_S$ , (14) is needed to calculate the scaling factor of the envelope detector.

For  $\lambda_{DSn} = \lambda_{DSp} = 0$ , (14) is simplified to

$$\frac{-1}{A_V} = \frac{n}{2} \frac{e^{-\frac{V_{DD} - V_{OUT}}{V_T}}}{1 - e^{-\frac{V_{DD} - V_{OUT}}{V_T}}} + \frac{n}{2} \frac{e^{-\frac{V_{OUT}}{V_T}}}{1 - e^{-\frac{V_{OUT}}{V_T}}}. \quad (15)$$

## D. Scaling Factor

As shown in (5), the scaling factor ( $k$ ) is related to  $A'_V$ , the first derivative of  $A_V$  with respect to  $A_V$  as

$$k = \frac{1}{2} \frac{dA_V}{dV_{IN}} = \frac{A'_V}{2}. \quad (16)$$

$A'_V$  can be obtained by 1) differentiating both sides of (14) with respect to  $V_{IN}$  and 2) simplifying the resulting equation as

$$A'_V = \frac{A_V^3}{V_T} \frac{n}{2} (\alpha - \beta), \quad (17)$$

where  $\alpha$  is

$$\alpha = \frac{e^{-\frac{V_{DD} - V_{OUT}}{V_T}}}{1 - e^{-\frac{V_{DD} - V_{OUT}}{V_T}}} \left( 1 + \frac{e^{-\frac{V_{DD} - V_{OUT}}{V_T}}}{1 - e^{-\frac{V_{DD} - V_{OUT}}{V_T}}} \right), \quad (18)$$

and  $\beta$  is

$$\beta = \frac{e^{-\frac{V_{OUT}}{V_T}}}{1 - e^{-\frac{V_{OUT}}{V_T}}} \left( 1 + \frac{e^{-\frac{V_{OUT}}{V_T}}}{1 - e^{-\frac{V_{OUT}}{V_T}}} \right). \quad (19)$$

$k$ , the scaling factor is

$$k = \frac{A_V^3}{V_T} \frac{n}{4} (\alpha - \beta). \quad (20)$$

The dependence of  $k$  on  $\lambda_{DS}$  is captured in (17) through  $A_V$ .  $G_V$ , the voltage conversion gain is a function of  $v_{in}$  and is

$$G_V = \frac{A_V^3}{V_T} \frac{n}{4} (\alpha - \beta) v_m. \quad (21)$$

## IV. RESULTS

### A. Transistor Parameters

Table I summarizes the transistor parameters used to generate characteristic curves for the VTC, the small signal gain, and the scaling factor of the inverter-based envelope detector.

TABLE I  
180-NM TRANSISTOR PARAMETERS.

Device	$n$	$I_o$ [ $\mu$ A]	$V_t^1$ [mV]	$\lambda_{DS}$
NMOS <sup>2</sup>	1.364	29.9	548.8	0.033
PMOS <sup>2</sup>	1.427	15.6	571.0	0.026

<sup>1</sup>  $V_t$  is extrapolated for  $V_{DS} = V_{BS} = 0$  V.

<sup>2</sup> The  $W/L$  ratios for the NMOS and the PMOS transistors are 1.0/0.18  $\mu$ m/ $\mu$ m and 1.37/0.18  $\mu$ m/ $\mu$ m, respectively.

### B. Voltage Transfer Characteristic

Figure 3 shows the simulated VTC and the calculated VTC. The VTC was simulated at the transistor-level using the BSIM4 model using Cadence Spectre. The calculated VTC was obtained by solving (12) using `fzero` in Matlab using transistor parameters from Table I. Since  $n_n \approx n_p$ ,  $n_n$  and  $n_p$  are averaged. An averaged  $n$  of 1.396 is used in the calculation.

The simulated  $V_S$  is 227 mV and the calculated  $V_S$  is 230 mV. The close agreement between the simulated and the calculated VTC suggests that in contrast to the VTC derived in [7], (12) accounts for the DIBL effect, yields a gradual descent near  $V_S$ , and accurately captures  $A_V$ .

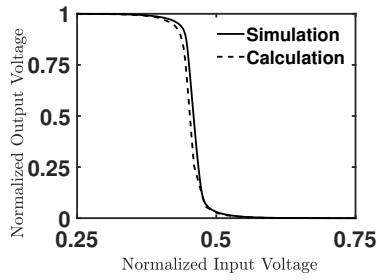


Fig. 3. Simulated and calculated VTC of an inverter cell. The input and output voltage are normalized to  $V_{DD}$  of 0.5 V.

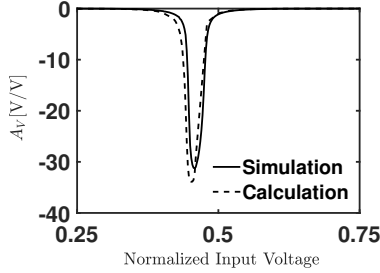


Fig. 4. The small signal voltage gain. The input voltage is normalized to  $V_{DD}$  of 0.5 V.

### C. Small Signal Voltage Gain

Figure 4 shows the simulated  $A_V$  and the calculated  $A_V$ . The calculated  $A_V$  was obtained by solving (14) with  $V_{OUT}$  from (12). The minimum of the simulated  $A_V$  is  $-32.36$  V/V and occurs at the normalized input voltage of 0.458. The minimum of the calculated  $A_V$  is  $-33.86$  V/V and occurs at the normalized voltage of 0.454.  $V_{DD}$  is 0.5 V. The close agreement between the simulated and the calculated  $A_V$  shows that in contrast to the small signal gain derived in [8], the expression derived in this article is accurate not only near the switching voltage, but also for any input voltage. More importantly, since the minimum and the maximum of second derivative of the voltage transfer function occur away from the switching voltage, a general small signal gain expression valid for any input voltage is needed to calculate the scaling factor of the envelope detector.

### D. Scaling Factor

Figure 5 shows the simulated and the calculated  $A'_V$ , the second derivative of the voltage transfer characteristic curve with respect to the input voltage. Since  $A'_V$  is equal to  $2k$ , where  $k$  is the scaling factor,  $A'_V$  is an indirect measure of  $k$ .

The calculated  $A'_V$  was obtained using (17). A close analysis of Fig. 5 shows that the minimum of calculated  $A'_V$  is  $-6,767$  1/V while that of the simulated  $A'_V$  is  $-7,476$  1/V. The percentage error of the minimum  $A'_V$  is  $-9.5\%$ . The maximum of calculated  $A'_V$  of  $4,779$  1/V occurs at  $3.0$  mV above  $V_S$  while that of the simulated  $A'_V$  of  $4,856$  1/V occurs at  $8.0$  mV above  $V_S$ . The percentage error of the minimum  $A'_V$  is  $-1.6\%$ . The close agreement between the simulated and the calculated

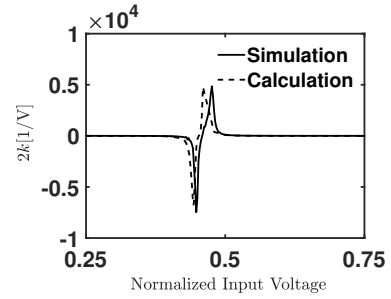


Fig. 5.  $A'_V$ , the second derivative of the voltage transfer characteristic curve with respect to the input voltage.  $A'_V$  is equal to  $2k$ , where  $k$  is the scaling factor.

$A'_V$  shows that the voltage conversion gain for an inverter-based envelope detector biased in the subthreshold region is accurately modeled using (17).

## V. CONCLUSION

This paper derives the formulas for the VTC, the small signal gain, and the scaling factor of the inverter-based envelope detector in the subthreshold region. The VTC expression produces a gradual descent near the switching voltage and accurately models the small signal gain. The small signal gain expression valid for any input voltage is needed to calculate the scaling factor or the conversion gain of the envelope detector. The close agreement between the simulated and the calculated results shows that the subthreshold inverter-based envelope detector is accurately modeled.

## REFERENCES

- [1] "Ericsson Mobility Report," Ericsson, June 2022. [Online]. Available: ericsson.com/mobility-report
- [2] K. W. Cheng and S. E. Chen, "An Ultralow-Power Wake-Up Receiver Based on Direct Active RF Detection," in *IEEE Transactions on Circuits and Systems I: Regular Papers*, vol. 64, no. 7, pp. 1661-1672, July 2017.
- [3] J. Ou, "On the Feasibility of an Inverter-Based CMOS Envelope Detector," 2022 65th Midwest Symposium on Circuits and Systems (MWS-CAS), 2022.
- [4] M. Zgaren and M. Sawan, "A Low-Power Dual-Injection-Locked RF Receiver With FSK-to-OOK Conversion for Biomedical Implants," in *IEEE Transactions on Circuits and Systems I: Regular Papers*, vol. 62, no. 11, pp. 2748-2758, Nov. 2015, doi: 10.1109/TCSI.2015.2477577.
- [5] L. Reyes and F. Silveira, "Gain, Signal-to-Noise Ratio and Power Optimization of Envelope Detector for Ultra-Low-Power Wake-Up Receiver," in *IEEE Transactions on Circuits and Systems II: Express Briefs*, vol. 66, no. 10, pp. 1703-1707, Oct. 2019, doi: 10.1109/TCSII.2019.2932767.
- [6] J. Ou and P. M. Ferreira, "A CMOS Envelope Detector for Low Power Wireless Receiver Applications," 2018 16th IEEE International New Circuits and Systems Conference (NEWCAS), 2018, pp. 44-47, doi: 10.1109/NEWCAS.2018.8585458.
- [7] S. M. Sharroush, "Analysis of the Subthreshold CMOS Logic Inverter," in *Ain Shams Engineering Journal*, no. 9, pp. 1001-1017, 2018, doi: 10.1016/j.asej.2016.05.005.
- [8] M. Alioto, "Understanding DC Behavior of Subthreshold CMOS Logic Through Closed-Form Analysis," in *IEEE Transactions on Circuits and Systems I: Regular Papers*, vol. 57, no. 7, pp. 1597-1607, July 2010, doi: 10.1109/TCSI.2009.2034233.
- [9] J. Yang and E. Skafidas, "A Low Power MICS Band Phase-Locked Loop for High Resolution Retinal Prosthesis," in *IEEE Transactions on Biomedical Circuits and Systems*, vol. 7, no. 4, pp. 513-525, Aug. 2013, doi: 10.1109/TBCAS.2012.2220545.